

# Unconsidered but influencing interference in unmanned aerial vehicle cabling system

Imas Tri Setyadewi<sup>1</sup>, Yanuar Prabowo<sup>1</sup>, Priyo Wibowo<sup>2</sup>, Purnomo Sidi Priambodo<sup>3</sup>

<sup>1</sup>Research Center for Aeronautics Technology, National Research and Innovation Agency, Bogor, Indonesia

<sup>2</sup>Research Center for Testing Technology and Standard, National Research and Innovation Agency, South Tangerang, Indonesia

<sup>3</sup>Department of Electrical Engineering, Universitas Indonesia, Depok, Indonesia

## Article Info

### Article history:

Received Apr 3, 2023

Revised Jul 12, 2023

Accepted Jul 17, 2023

### Keywords:

Cable

Interference

Polarization

Radiation

Unmanned aerial vehicle

## ABSTRACT

The increasing complexity of electrical and electronic systems in unmanned aerial vehicles (UAVs) has raised concerns regarding unwanted electromagnetic interference (EMI) due to limited compartment space. Recent studies have highlighted the UAV cabling as the primary pathway for interference. This paper presents a novel approach to investigating the effects of interference power, polarization angle, and distance from the interference source on EMI in UAV cable systems. Measurements and simulations were performed to analyze the influence of these factors on the radiation received by the cable. A linear dipole antenna, operating at a frequency of 905 MHz, served as the radiation source, while a single wire cable pair terminated with a 50-ohm resistor was employed as the victim. The findings reveal that the power transmitted by the source, the distance between the cable and the source, and the polarization angle have a significant impact on the electromagnetic interference received by the cable. Notably, a perpendicular orientation of the cable to the interference source (antenna) in the far-field yielded a reduction of up to 15 dBm in EMI. The results underscore the necessity for more sophisticated models and comprehensive measurements to fully comprehend the diverse factors affecting polarization losses in practical scenarios.

This is an open access article under the [CC BY-SA](https://creativecommons.org/licenses/by-sa/4.0/) license.



## Corresponding Author:

Purnomo Sidi Priambodo

Department of Electrical Engineering, Universitas Indonesia

Depok 16424, West Java, Indonesia

Email: purnomo.sidhi@ui.ac.id

## 1. INTRODUCTION

The development of information technology and electronics in unmanned aerial vehicles (UAVs) has led to increasingly complex electrical and electronic systems [1]. However, the limited compartment space in UAVs poses a potential source of unwanted electromagnetic interference (EMI) [2]–[4]. Previous research has shown that 60% of EMI occurrences on aircraft are caused by electromagnetic interference coupled to UAV wiring systems [5]. Cable length has been identified as a major factor influencing the electromagnetic susceptibility of devices to EMI, both from internal and external sources [2], [6]–[9]. The interference problem in UAVs is increasingly complex due to the structure of the UAV body, which is generally made of lightweight and strong composites, providing a fairly good level of flexibility compared to metal. This UAV structure offers flexibility but is less effective at withstanding electromagnetic interference compared to metal materials [7], [10].

Several research studies have investigated methods for predicting radiated emission from cables and reducing EMI. One such approach involves utilizing the simplified simulation program with an integrated

circuit emphasis (SPICE) model [11]. The result estimates the amount of emission (current) received by cables starting from the frequency range of 60 MHz to 1 GHz in the vertical antenna polarization direction [12]. Another method focuses on reducing the radiation absorbed by printed circuit boards (PCBs) in the far-field at a distance of 1 meter, achieved by incorporating a smart patch loop on the PCB, resulting in an average emission reduction of 83% [13]. However, this method can only be applied to integrated circuit (IC) circuits.

Investigations have also been conducted to explore the impact of radiation on different types of cables at varying distances from the source [14]. Using a radiation source from a supply cable with an input signal of 10 V at a frequency of 2 MHz, the amount of crosstalk in the receiving cable was analyzed by adjusting the distance from 1 to 10 cm. The results show that distances exceeding 4 cm from the source can reduce the amount of EMI received by up to 60% [14]. Additionally, cables with copper shields demonstrated a 50% reduction in EMI at a distance of 1 cm compared to cables without shields [15].

A measurement of radiated electromagnetic emission using a shielded cable by varying the height of the cable to the ground has been conducted. Parameters that affect emissions, such as current distribution, dielectric properties of the ground (reflection coefficient), and reflected current on the cable, were considered [3]. As a result, this measurement model can be used to predict emissions from shielded cables on certain ground materials, but the distance factor of the cable to the source has yet to be determined.

Similarly, Park *et al.* [16] developed a measurement method by simplifying the estimation of common mode radiation from a cable connected to a real device, which is a mobile device, by measuring the common mode current. The simulation is carried out by modeling a mobile device like a conducting box. The equivalent source between the conducting box and the power cable can be determined by measuring the common mode current in the cable, which contains all the noise coupled to the body of the mobile device [16]. This measurement can only be used at frequencies below 300 MHz to estimate EMI at the radiation peak.

Although previous studies have explored methods to mitigate interference in UAV systems, the effects of cable distance and polarization angle have not been adequately addressed. Therefore, this paper proposes an alternative approach to investigate and analyze the effects of these two factors, comparing the results obtained from measurements and simulations. Understanding the influence of cable distance and polarization angle will provide valuable insights for designing UAV cable line systems and configuring onboard equipment to effectively mitigate interference effects on UAV system operation.

## 2. METHODS

### 2.1. Measurement setup

Figure 1 illustrates the setup used for measuring electromagnetic radiation emission. The measurements were conducted in a semi-anechoic chamber, where the antenna was placed at various distances ( $L$ ) based on the characteristics of the wave impedance. These distances included the near-field at 0.1 m, Fresnel at 0.33 m, and far-field at 1 m away from the cable under test (CUT). The calculation of the near-field, Fresnel, and far-field was based on the wavelength ( $\lambda$ ) and length of the antenna [17]. The VERT dipole antenna was used, with an operating working frequency of 824 to 960 MHz. For this study, a frequency of 905 MHz was chosen as it is widely used for UAV working frequencies.

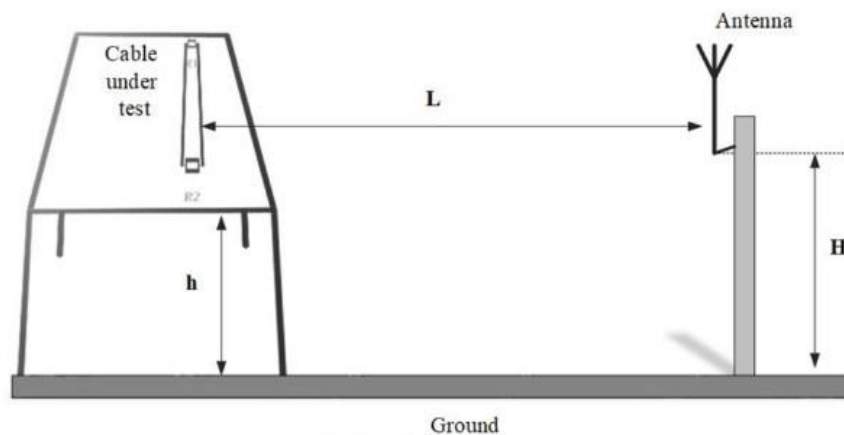


Figure 1. Radiation test setup

To measure the variation in polarization angle, the antenna was positioned at different angles from the cable [18]. This included  $90^\circ$ , which means perpendicular to the cable, at  $45^\circ$  and  $0^\circ$  in a horizontally laid position with the cable. The cable used was a single wire cable pair, 0.7 m long, and had a resistance of 50 Ohms at each end. The cable was placed horizontally on a foam table with a height of (h) 1 m above the ground chamber. The FieldFox microwave spectrum analyzer N9917A was connected to the other end of the cable as an instrument reader output. The transmit power of the EXG Keysight N5173B analog signal generator to the antenna was varied from -19 to 20 dBm in increments of 5 dB on both vertical and horizontal polarization antennas.

The magnitude of the radiation intensity received in the far-field was measured in the form of a power receive ( $P_r$ ). The amount of power received was calculated as stated in (1).

$$P_r = e_r D_r(\theta_r, \phi_r) \frac{\lambda^2}{4\pi} P_D \quad (1)$$

$e_r$  is the radiation efficiency of the receiving antenna, where  $D_r$  is the directivity receiving antenna in the direction  $\theta_r, \phi_r$ , and power density ( $P_D$ ) is calculated using (2).

$$P_D = \frac{P_t G_t(\theta_t, \phi_t)}{4\pi R^2} \quad (2)$$

where  $P_t$  is the transmit power,  $G_t$  is the gain of the transmitting antenna in the direction  $\theta_t, \phi_t$ , and  $R$  is the distance between the transmitting and receiving antenna [19]. The power received represented in (1) assumes that the transmitting and receiving antennas were matched, and the polarization of the receiving antenna was the same as the transmitted polarization.

## 2.2. Cable simulation

Cable simulation using the computer simulation technology (CST) Cable Studio has been conducted to compare with the value obtained by laboratory measurements. The simulation was carried out at a far-field distance by using a plane wave as a radiation source. The magnitude of the electric field intensity (V/m) was calculated using (3).

$$P_D = \frac{E^2}{z_0} = \frac{E^2}{120\pi} = \frac{E^2}{377} \quad (3)$$

The magnitude of the electric field ( $E$ ) was obtained by multiplying the power density ( $P_D$ ) parameter received based on the calculation with the air impedance in the field area. In the far-field, the air impedance is equivalent to 377 ohms or the value of the impedance with space impedance is the same ( $z_0 = z_w$ ). In the near-field, the impedance ( $z_w$ ) is a function of distance, as shown in Figure 2, so (4) can be used [17], [20], [21]. Using (4) and refers to Figure 2, a  $z_w$  value of each field can be obtained.

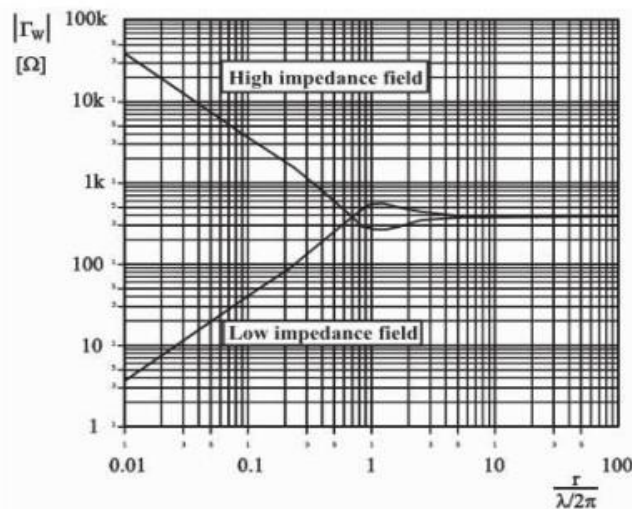


Figure 2. Field impedance as a function of distance

$$z_W = z_0 \left( \frac{\lambda}{2\pi r} \right) \quad (4)$$

The simulation used schematic circuits that were identical to the measurement configuration in the chamber, as shown in Figure 3. A plane wave was used as a radiation source by providing  $z_W$  input according to the field area. The simulation results were expressed in the form of power induction received by the cable in dBW.

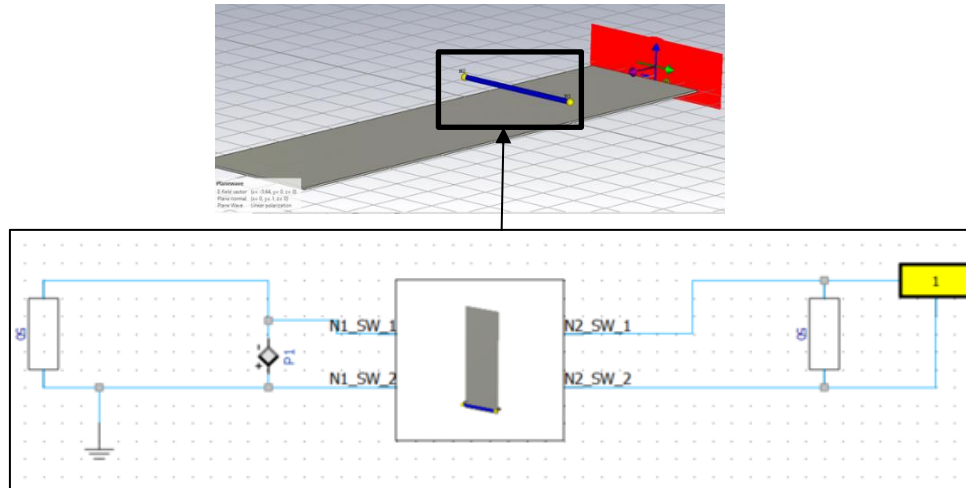


Figure 3. Schematic diagram in CST cable studio

### 3. RESULTS AND DISCUSSION

#### 3.1. Measurement radiated susceptibility of cable

The electromagnetic interference was measured by varying the transmitting power of the dipole antenna source at polarization angles of  $0^\circ$ ,  $45^\circ$ , and  $90^\circ$  over a 0.7 m length of cable that was laid on a table in the horizontal direction, as shown in Figure 1. The frequency source was set to 905 MHz, and the measurement results were monitored by the spectrum analyzer and analyzed by comparing them with the simulation. The measurement results are shown in Figure 4.

Figure 4(a) shows the values of the power radiation received by the cable when the distance between the cable and the source was 0.1 m or in the near-field area. Meanwhile, the radiation received value by the cable at a distance of 0.33 m or in the Fresnel zone area was shown in Figure 4(b), and the radiation in the far-field area was shown in Figure 4(c). The Y-axis represents the amount of radiation received by the cable, while the X-axis represents the power transmitted to the antenna ranging from -20 to 19 dBm with an increment interval of 5 dBm. From the overall results obtained, it was observed that there was a linear relationship between the transmitted power of the source and the radiation received by the cable. An increase in transmit power led to an increase in the amount of radiation received by the cable, which was in accordance with (1) and (2). Therefore,  $P_r$  was linear to  $P_t$ . For every 5 dBm increase given on the cable, an average increase of 4.8 dBm was obtained.

The influence of distance on electromagnetic interference received by the cable was found to be significant, particularly at distances above 0.33 m. The maximum radiation values of -19.36 and -20.9 dBm were observed at the Fresnel and far-field distances, respectively, in the polarization direction of  $0^\circ$  (square symbol). Conversely, the highest radiation was recorded at the near-field distance with a polarization angle of  $90^\circ$  (triangle symbol), reaching -12.5 dBm. It was observed that increasing the distance between the cable and the source resulted in a linear negative relationship, causing a decrease in the radiation received by the cable. This relationship was expressed by (1), which demonstrated that in the far-field, the radiation received decreased quadratically as a function of the distance from the source. The calculations revealed that the magnitude of radiation received was within acceptable limits, decreasing quadratically in proportion to the emitted power, as indicated by the equation for a radiation magnitude of 19 dBm in Figure 4(c). However, this trend did not apply to the polarization direction of  $90^\circ$ , where the highest radiation value was obtained at the near-field distance. Furthermore, the radiation value at a polarization angle of  $90^\circ$  was found to be significantly lower in the far-field region, with a difference of up to 15 dBm compared to the near-field distance.

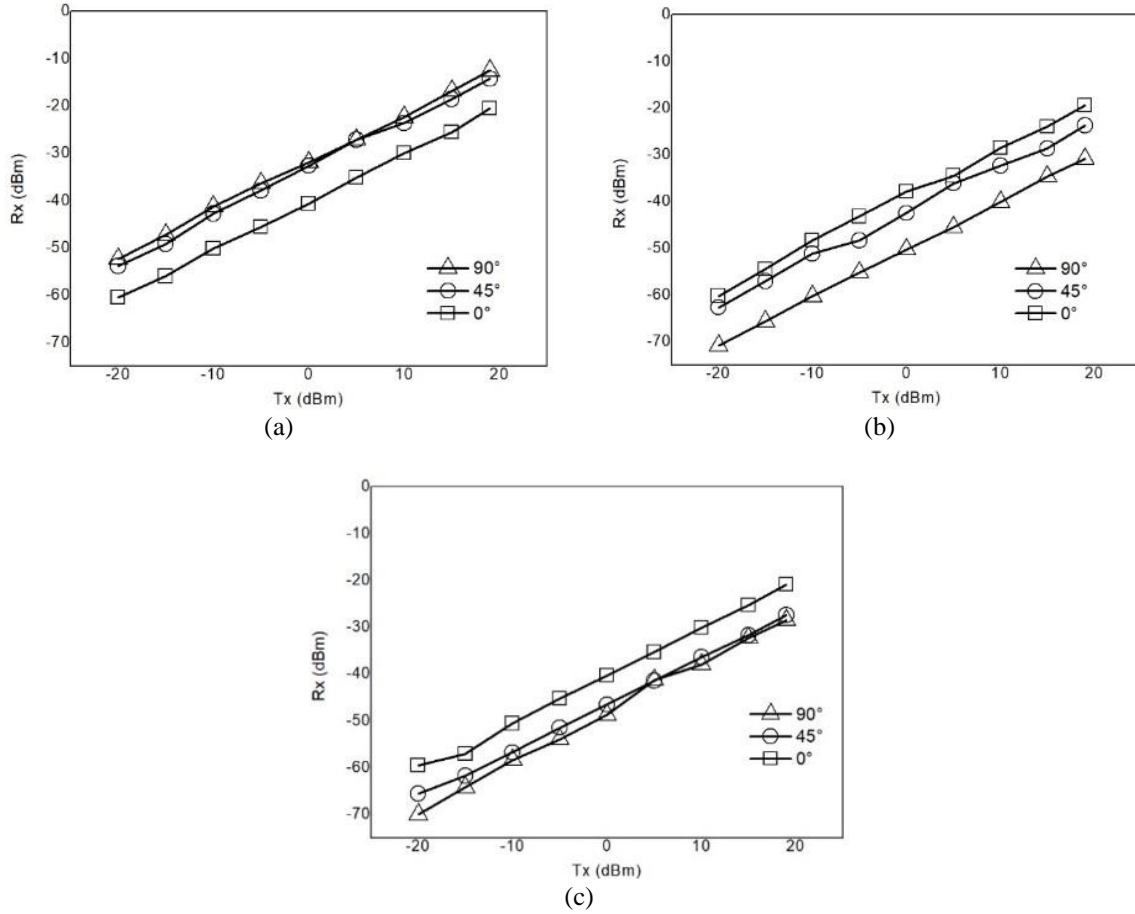


Figure 4. Interference received by cable at (a) near-field 0.1 m, (b) Fresnel 0.33 m, and (c) far-field 1 m

The findings highlight the importance of considering cable distance and polarization angle in EMI analysis. The influence of antenna polarization can be analyzed based on the polarization loss factor (PLF) equation, where the polarization mismatch causes the power received by the receiving antenna to be less than the maximum. Polarization losses can be defined as the magnitude of the cosine vector angle between the wave vector and its polarization vector. The PLF equation is given by (5) [19].

$$PLF = |\hat{\rho}_\omega \cdot \hat{\rho}_a|^2 = |\cos \psi_p|^2 \quad (5)$$

where  $\hat{\rho}_\omega$  is a wave unit vector,  $\hat{\rho}_a$  is a polarizing vector and  $\psi_p$  is the angle between the two vector units. If the angles of the two vectors meet, which means they form an angle of  $0^\circ$ , then the magnitude of the PLF in decibels (dB) will be zero (7). This is because the electric field of the antenna will be oriented in the same direction as the conductors in the cable, resulting in a stronger coupling between the antenna and the cable.

$$PLF = |\cos 0|^2 = 1 \quad (6)$$

$$PLF (dB) = 10 \log_{10} PLF = 0 \quad (7)$$

If the polarization angle is  $45^\circ$  (circle symbol), then the loss factor is 3 dB. Figures 4(b) and 4(c) demonstrate the connection between polarization and the amount of energy received, which was smaller at  $45^\circ$  polarization than at  $0^\circ$  polarization. The radiation received was smaller by an average of 5 dBm. When the distance to the source was 0.3 m in the Fresnel zone, the radiation output at a  $45^\circ$  angle was closer to the same result as the  $0^\circ$  angle, but when the distance was 1 m, it shifted closer to the same polarization value as the  $90^\circ$  angle. Based on (6) and (7), if the PLF angle was  $90^\circ$ , then the loss factor became infinite. This is because the electric field of the antenna will be oriented perpendicular to the conductors in the cable, resulting in a weaker coupling between the antenna and the cable [22].

This behavior can be explained by a decrease in the dominance of one of the fields, either magnetic (H) or electric (E) field, as shown in Figure 5. As the distance approaches the far-field, the E and H values will converge to the same value, forming a plane wave. The field in the Fresnel zone has a large attribute where the electric field and magnetic field almost resemble plane waves, but there is still some influence of field reflection from the near-field. In contrast, when compared to radiation received in the near-field, the greatest polarization is received at an angle of  $90^\circ$  or perpendicular to the cable. In the near-field, one of the field components dominates, and the waveform is not in phase and does not form a plane wave. Therefore,  $90^\circ$  polarization produces a larger value which could be due to the higher magnetic field (H) in that area compared to the electric field (E) [20].

### 3.2. Simulating the polarization effect

To establish a relationship between the measurement parameters and ideal simulation values, simulations were conducted to estimate the radiation received by the cable. The electric field intensity obtained from the power density calculation in (1) was used to determine the magnitude of the intensity in the far-field. This value served as an input for the field intensity in the simulations, which were performed using plane waves at an antenna polarization angle of  $0^\circ$ . This configuration ensured that the electric field direction was parallel to the cable. The simulations were conducted at a far-field distance of 1 meter, as (1) specifically applies to the far-field region. Therefore, the electric field intensity value assigned to the plane wave was only valid for the far-field distance [19].

The simulations conducted in this study focused on a transmit power range of 0 to 19 dBm. This range was chosen due to the linear relationship observed in the simulation values, enabling reliable predictions. Thus, within this range, it was expected that a correlation could be established between the measured values and the simulation results. Figure 5(a) illustrates that the simulations exhibited similar trends to the measurements, indicating that higher transmit power resulted in increased radiation received by the cable at polarization angles  $0^\circ$  and  $45^\circ$ . However, at a polarization angle of  $90^\circ$ , there was a notable difference in the power received by the cable between the simulation and measurement results, as depicted in Figure 5(b).

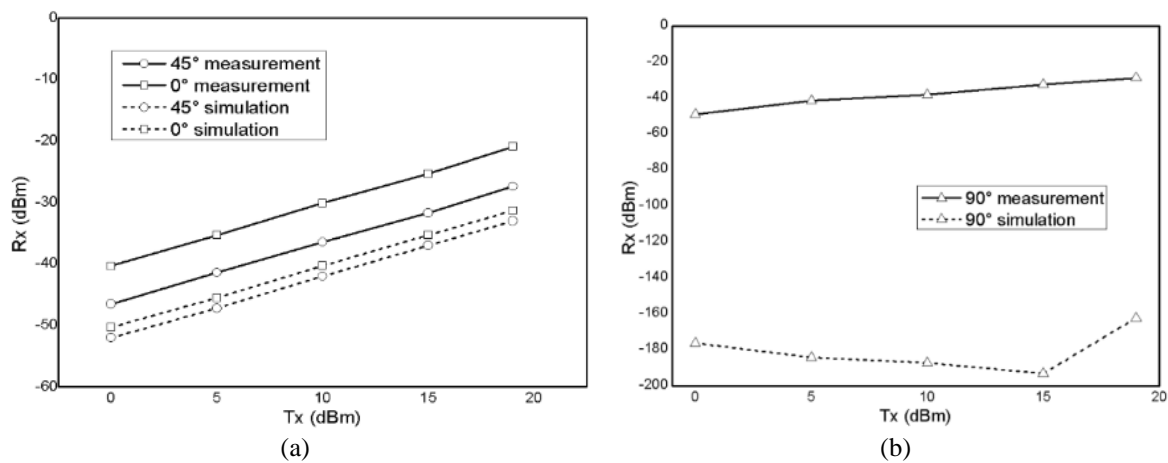


Figure 5. Measurement vs simulation in far-field at (a) polarization angle  $0^\circ$ ,  $45^\circ$ , and (b)  $90^\circ$

The simulation results aligned with the PLF equation, which suggests that the power received by the cable is reduced due to weaker coupling between the antenna and the cable caused by polarization mismatch. Conversely, the measurement results also indicated that power coupling still occurred from the antenna to the cable. It is important to acknowledge that the PLF equation assumes idealized conditions and may not fully capture all the factors influencing polarization losses in real-world scenarios [19]. Antenna polarization and its impact on electromagnetic interference can be influenced by various factors, such as the environment, multipath propagation, and antenna characteristics. Therefore, a practical analysis of polarization losses often requires more complex models and measurements.

Furthermore, when analyzing electromagnetic interference and polarization effects in practical scenarios, additional factors and techniques need to be considered. The simulations accounted for cable connectors and reflections, which can affect the overall measurement value [23]. Additionally, the simulations utilized plane waves as a source without considering correction factors for the antenna's radiation

pattern. As a result, reflections, whether phased or unphased, can either enhance or weaken the power received by the cable. Some reflections may interfere with the original wave, leading to constructive or destructive interference. When a plane wave encounters the cable, reflections can occur, influencing the cable's received power based on the phase and amplitude of the reflected wave.

To address these factors, correction factors may be incorporated into the antenna's radiation pattern through measurements or simulations that consider the reflections and environmental geometry. These correction factors improve the accuracy of the simulations and account for the impact of reflections on the received power [24]–[27]. By integrating correction factors into the simulations, inaccuracies can be mitigated, leading to enhanced overall accuracy of the results. When simulating the performance of a cable receiving a plane wave from a real antenna, it is crucial to consider the possibility of reflections and incorporate appropriate correction factors to ensure more reliable and accurate outcomes [28].

#### 4. CONCLUSION

In this study, a comprehensive analysis of the electromagnetic radiation effects on UAV cable systems was presented, considering transmit power, polarization angle, and distance from the interference source. The measurement results demonstrated a linear relationship between the transmitted power of the source and the radiation received by the cable. The results revealed that multiple variables significantly influenced the amount of electromagnetic radiation received by the cable. Moreover, the impact of the polarization angle varied between the near-field and far-field regions. In the near-field region, the greatest radiation was received when the polarization angle was perpendicular to the cable, whereas, in the far-field, the greatest radiation was received when the polarization angle matched the cable.

The findings highlighted the importance of considering cable distance and polarization angle in EMI analysis. The PLF equation provided insights into the impact of antenna polarization on the power received by the cable. The simulations and measurements showed that the PLF equation was applicable, with polarization mismatch resulting in a reduction in the power received by the cable. However, the measurements also indicated that power coupling still occurred from the antenna to the cable, suggesting additional factors influencing polarization losses in real-world scenarios. To improve the accuracy of simulations, correction factors are suggested to be applied to the antenna's radiation pattern, taking into account the possibility of reflections.

Overall, understanding the effects of cable distance, polarization angle, and reflection phenomena is essential for designing UAV cable line systems and configuring onboard equipment to effectively mitigate EMI and ensure optimal system operation. Future research should consider more complex models and measurements to capture the diverse factors influencing polarization losses in practical scenarios.

#### ACKNOWLEDGEMENTS

This work was supported by the National Agency for Research and Innovation (BRIN) of the Republic of Indonesia, which provided material support and the opportunity for the authors to conduct and complete the research.

#### REFERENCES

- [1] Y. Prabowo, N. Chasanah, and A. N. Jati, "Design of reflector microstrip patch antenna for LAPAN surveillance UAV (LSU) application," *Journal of Physics: Conference Series*, vol. 1130, Nov. 2018, doi: 10.1088/1742-6596/1130/1/012019.
- [2] S. V Averin, V. Y. Kirillov, E. V Mashukov, S. B. Reznikov, and D. A. Shevtsov, "Ensuring the electromagnetic compatibility of onboard cables for unmanned aerial vehicles," *Russian Aeronautics*, vol. 60, no. 3, pp. 442–446, 2017, doi: 10.3103/S1068799817030175.
- [3] A. T. Baklezos, C. D. Nikolopoulos, A. G. Katsouris, G. I. Koutantos, and C. N. Capsalis, "Electromagnetic emission modeling in case of shielded cabling with respect to the ground dielectric properties," *IEEE Transactions on Electromagnetic Compatibility*, vol. 58, no. 6, pp. 1694–1700, 2016, doi: 10.1109/TEM.2016.2588583.
- [4] R. R. Gainutdinov and S. F. Chermoshentsev, "Methodology to ensure the intrasystem electromagnetic compatibility of UAV avionics," *Russian Aeronautics*, vol. 59, no. 4, pp. 613–618, 2016, doi: 10.3103/S1068799816040279.
- [5] Y. WU and Q.-S. MA, "Progress of electromagnetic compatibility design for unmanned aerial vehicles," *DEStech Transactions on Engineering and Technology Research*, 2019, doi: 10.12783/dtetr/icicr2019/30548.
- [6] A. Tsaliovich, "Cable shielding for electromagnetic compatibility," *Cable Shielding for Electromagnetic Compatibility*, 1995, doi: 10.1007/978-1-4615-6591-8.
- [7] H. Shakhathreh, A. H. Sawalmeh, A. L. A. Al-fuqaha, S. Member, and Z. Dou, "Unmanned aerial vehicles (UAVs): a survey on civil applications and key research challenges," *IEEE Access*, vol. 7, pp. 48572–48634, 2019, doi: 10.1109/ACCESS.2019.2909530.
- [8] V. H. Céspedes, L. Fernando, D. Cadavid, Y. Alberto, and G. Gómez, "Electromagnetic pollution maps as a resource for assessing the risk of emissions from mobile communications antennas," *International Journal of Electrical and Computer Engineering (IJECE)*, vol. 10, no. 4, pp. 4244–4251, 2020, doi: 10.11591/ijece.v10i4.pp4244-4251.

- [9] P. Wibowo, H. Dwi Prananto, Yudhistira, Yoppy, M. K. Anam, and R. H. Arjadi, "Characterization of electromagnetic compatibility performance of trains LED lighting by mapping of radiated interference distribution," in *2017 International Multidisciplinary Conferences on Productivity and Sustainability*, 2017, pp. 39–42.
- [10] R. Turczyn, K. Krukiewicz, A. Katunin, J. Sroka, and P. Sul, "Fabrication and application of electrically conducting composites for electromagnetic interference shielding of remotely piloted aircraft systems," *Composite Structures*, vol. 232, Art. no. 111498, 2020, doi: 10.1016/j.compstruct.2019.111498.
- [11] M. Raya and R. Vick, "Spice models of shielded single and multiconductor cables for emc analyses," *IEEE Transactions on Electromagnetic Compatibility*, vol. 62, no. 4, pp. 1563–1571, 2020, doi: 10.1109/TEMC.2020.3006391.
- [12] G. Li *et al.*, "Prediction of radiated emissions from cables over a metal plane using a SPICE model," *IEEE Transactions on Electromagnetic Compatibility*, vol. 57, no. 1, pp. 61–68, 2015, doi: 10.1109/TEMC.2014.2364405.
- [13] M. Koohestani, M. Ramdani, and R. Perdriau, "Reduction of radiated far-field emission and susceptibility using a suspended metal loop," *Proceedings of the 2020 International Symposium on Electromagnetic Compatibility - EMC EUROPE, EMC EUROPE 2020*, pp. 8–11, 2020, doi: 10.1109/EMCEUROPE48519.2020.9245726.
- [14] R. R. Gaynutdinov and S. F. Chermoshentsev, "Study of crosstalks in the cables of unmanned aerial vehicle," in *2017 International Siberian Conference on Control and Communications (SIBCON)*, 2017, pp. 1–4, doi: 10.1109/SIBCON.2017.7998540.
- [15] I. T. Setyadewi and P. S. Priambodo, "Study and analysis of crosstalk reduction in UAV cabling by using various cable types," *Evergreen*, vol. 9, no. 1, pp. 150–155, 2022, doi: 10.5109/4774232.
- [16] H. H. Park, H. B. Park, and H. S. Lee, "A simple method of estimating the radiated emission from a cable attached to a mobile device," *IEEE Transactions on Electromagnetic Compatibility*, vol. 55, no. 2, pp. 257–264, 2013, doi: 10.1109/TEMC.2012.2219587.
- [17] H. W. Ott, *Electromagnetic compatibility engineering*. John Wiley & Sons, Inc., 2009.
- [18] D. Zhang, E. Cheng, H. Wan, X. Zhou, and Y. Chen, "Prediction of electromagnetic compatibility for dynamic datalink of UAV," *IEEE Transactions on Electromagnetic Compatibility*, vol. 61, no. 5, pp. 1474–1482, 2019, doi: 10.1109/TEMC.2018.2867641.
- [19] C. Balanis, *Antenna theory*. wiley, 2010.
- [20] K. H. Gonschorek and R. Vick, "Electromagnetic compatibility for device design and system integration," *Electromagnetic Compatibility for Device Design and System Integration*, pp. 1–470, 2009, doi: 10.1007/978-3-642-03290-5.
- [21] C. J. Robert F., D. M. Sylvar, and J. L. Ulcek, "Evaluating compliance with FCC guidelines for human exposure to radiofrequency electromagnetic fields," *FCC OET Bulletin 65*, no. August, pp. 1–79, 1997, doi: 10.1109/isemc.2004.1349969.
- [22] Gershon J. Wheeler, *Introduction to microwave*, vol. 7, no. 2. America: Prentice-Hall, 1963.
- [23] J. Song, H. T. Hui, and Z. W. Sim, "Investigation of measurement uncertainties and errors in a radiated emission test system," *IEEE Transactions on Electromagnetic Compatibility*, vol. 57, no. 2, pp. 158–163, 2015, doi: 10.1109/TEMC.2014.2366163.
- [24] B. M. Kolundzija, "Electromagnetic modeling of composite metallic and dielectric structures," *IEEE Transactions on Microwave Theory and Techniques*, vol. 47, no. 7, pp. 1021–1032, 1999, doi: 10.1109/22.775434.
- [25] S. Piersanti *et al.*, "Near-Field shielding performances of EMI noise suppression absorbers," *IEEE Transactions on Electromagnetic Compatibility*, vol. 59, no. 2, pp. 654–661, 2017, doi: 10.1109/TEMC.2016.2626299.
- [26] J. Ala-Laurinaho, Z. Du, V. Semkin, V. Viikari, and A. V. Raisanen, "Reflection coefficient method for antenna radiation pattern measurements," *2015 European Radar Conference, EuRAD 2015 - Proceedings*, pp. 285–288, 2015, doi: 10.1109/EuRAD.2015.7346293.
- [27] B. M. Kolundzija and A. Djordjevic, *Electromagnetic modeling of composite metallic and dielectric structures*. Norwood: Artech House antennas and propagation library, 2002.
- [28] A. Sakonkanapong and C. Phongcharoenpanich, "Near-field HF-RFID and CMA-based circularly polarized far-field UHF-RFID integrated tag antenna," *International Journal of Antennas and Propagation*, vol. 2020, 2020, doi: 10.1155/2020/6427157.

## BIOGRAPHIES OF AUTHORS



**Imas Tri Setyadewi**    received a B.Sc. degree in physics, Faculty of Mathematics and Science, in 2012 and a master's degree in electrical engineering with a major in electronics and smart embedded systems in 2022 from Universitas Indonesia (UI). She has been working in the government sector at the National Research and Innovation Agency (BRIN) as UAV Engineer since 2014. Her research interest includes electromagnetic field, electrical system, avionics, and UAV propulsion. She can be contacted at email: imas003@brin.go.id, imas.3setya@gmail.com.



**Yanuar Prabowo**    was born in Surabaya, Indonesia, He obtained a Bachelor's degree in electrical engineering in 2008 from Institut Teknologi Sepuluh Nopember (ITS), Surabaya, Indonesia, and a master's degree in electrical engineering with a major in telecommunication engineering in 2017 from Universitas Indonesia in Depok, Indonesia. He has worked as a researcher at National Research and Innovation Agency, at the Aeronautics and Space Research Organization at BRIN since 2010. His research interest includes datalink communications, avionics, antennas, and RF components. He can be reached via email: yanu004@brin.go.id.



**Priyo Wibowo**    received a B.Eng. degree in physics from Yogyakarta State University, Yogyakarta, Indonesia, in 2004, and a master's degree in electrical engineering, specializing in telecommunications engineering from the University of Indonesia, Depok, Indonesia. He has experience working as the technical manager at the Electromagnetic Laboratory of the Indonesian Institute of Science. He is currently a researcher at the National Research and Innovation Agency, at the Research Center for Testing Technology. His current research interest includes applied electromagnetics, electromagnetic compatibility, testing technology, instrumentation, telecommunications, and antennas. He can be contacted at email: priyo.wibowo@brin.go.id.



**Purnomo Sidi Priambodo**    (IEEE M'1996) received his BS in electrical engineering from Universitas Gadjah-Mada, Indonesia 1987. From 1987 to 1994, he joined PT Indosat, experiences from satellite earth stations to data communication and system programming. MS degree from the School of Electrical and Computer Engineering, Oklahoma State University at Stillwater in 1996. A doctoral degree in photonics from the Department of Electrical Engineering at the University of Texas at Arlington, USA in 2003. Dr. Priambodo has been a member of the IEEE Lasers and Electro-Optics Society (LEOS) since 1996. He is also a member of the honor societies of Eta Kappa Nu and Phi Beta Delta. Dr. Priambodo's research interests include renewable-energy storage, medical photonics, free-space optical communications, and optical filters. He joined the Department of Electrical Engineering, Universitas Indonesia in 2007 and since 2017, Dr. Priambodo has held a position as an associate professor in optoelectronics engineering at the same university. He can be contacted at email: purnomo.sidhi@ui.ac.id.